ARTICLES

MAPK-mediated bimodal gene expression and adaptive gradient sensing in yeast

Saurabh Paliwal[1], Pablo A. Iglesias[1,2], Kyle Campbell[3], Zoe Hilioti[1], Alex Groisman[3] & Andre Levchenko[1]

The mating pathway in *Saccharomyces cerevisiae* has been the focus of considerable research effort, yet many quantitative aspects of its regulation still remain unknown. Using an integrated approach involving experiments in microfluidic chips and computational modelling, we studied gene expression and phenotypic changes associated with the mating response under well-defined pheromone gradients. Here we report a combination of switch-like and graded pathway responses leading to stochastic phenotype determination in a specific range of pheromone concentrations. Furthermore, we show that these responses are critically dependent on mitogen-activated protein kinase (MAPK)-mediated regulation of the activity of the pheromone-response-specific transcription factor, Ste12, as well as on the autoregulatory feedback of Ste12. In particular, both the switch-like characteristics and sensitivity of gene expression in shmooing cells to pheromone concentration were significantly diminished in cells lacking Kss1, one of the MAP kinases activated in the mating pathway. In addition, the dynamic range of gradient sensing of Kss1-deficient cells was reduced compared with wild type. We thus provide unsuspected functional significance for this kinase in regulation of the mating response.

The pheromone sensing MAPK pathway in the yeast *S. cerevisiae* affects the expression of an estimated 200 genes and directly participates in yeast chemotropism in pheromone gradients[1]. The pheromone response involves the formation of a diploid zygote from two haploid cells of opposite mating types through pheromone gradient sensing, directed localized cell growth (shmooing) and eventual cell fusion, and requires an integrated regulatory network. In spite of a long and productive research history, the control mechanisms involved in pheromone gradient sensing and chemotropism are still not completely understood. For example, it is not clear how the mean value and the gradient of the pheromone concentration are integrated by a chemotropic cell, whether the dose response in this pathway is graded, as suggested by a recent analysis[2], or switch-like, as observed in other MAPK cascades[3], and whether the response is affected by molecular-level noise. In addition, the respective roles of two MAP kinases activated by the pathway, Fus3 and Kss1, remain unclear.

Microfluidic chip-based experimental platform

To perform repeated high-throughput experiments on yeast pheromone response in precisely defined gradients, we developed a novel microfluidic device (Fig. 1a, b; Supplementary Fig. 1). Its functional area consists of an array of 5-μm-deep parallel rectangular test chambers of various lengths (short horizontal channels in Fig. 1a, b) and two 25-μm-deep mirror-symmetric flow-through channels adjacent to opposite edges of the test chambers (long vertical channels with kinks in Fig. 1a, b). Cells loaded into the test chambers are exposed to linear concentration profiles of pheromone (Supplementary Fig. 2). The pheromone gradient profiles are created by molecular diffusion between the left flow-through channel with a high concentration pheromone solution and the right flow-through channel with plain medium. In contrast to a previous microfluidic design for experiments on gradient response[4], cells in the test chambers are not exposed to any active flow, which is critical for experiments with non-adherent yeast cells. The pheromone gradient profiles in the test chambers remain stable over at least 20 h. A single microfluidic device contains multiple copies of test chambers of different lengths, allowing exposure of cells to a continuous range of pheromone concentrations presented in gradients of different steepness, as well as analysis of hundreds of cells per experiment. Therefore, long-term pheromone dose and gradient responses of individual cells can be analysed at high throughput. In addition, the cell phenotype and the expression level of specific fluorescently tagged genes can be monitored concurrently, an important capability unachievable with flow cytometry.

Phenotype co-existence versus bimodal gene expression

We used the device to study the phenotypic dose response of individual cells to pheromone concentration, c_{ph}, gradually varying from 0–80 nM. Although cell response was tracked continuously, the final analysis was performed six hours after pheromone exposure to reduce the effect of cell cycle stage variability at the beginning of the experiment. Specifically, cells past the G1-stage on pheromone exposure had sufficient time to complete their cell cycles and then attain their eventual phenotypic states. At six hours, cells adopted a variety of pheromone response phenotypes. At relatively high c_{ph}, cells formed multiple mating projections or exhibited prolonged chemotropism ('shmooing' or SHM phenotype), whereas at lower c_{ph} they underwent cell cycle arrest without formation of a shmoo (CCA phenotype). At yet lower c_{ph}, they showed no detectable response and continued dividing ('budding' or BUD phenotype)[5]. Additionally, some cells reverted from the SHM to the BUD phenotype ('reverted from shmooing' or RFS phenotype; see Supplementary Methods for cell phenotype determination). Surprisingly, distinct phenotypes often co-existed in cell subpopulations exposed to the same c_{ph} (Fig. 1e–g, i), indicating the existence of a range of c_{ph}, where the decision to acquire a specific phenotype might depend on stochastic features of the underlying biochemical reactions.

To gain insight into the phenotype co-existence, we generated cells expressing Fus3 and Fus1 proteins fused to yeast enhanced green

[1]Department of Biomedical Engineering and Whitaker Institute of Biomedical Engineering, and [2]Department of Electrical Engineering and Computer Engineering, The Johns Hopkins University, Baltimore, Maryland 21218, USA. [3]Department of Physics, University of California, San Diego, La Jolla, California 92093, USA.

fluorescent protein (EGFP), Fus3–EGFP and Fus1–EGFP, by genomic integration of *EGFP* at the respective native loci (referred to as wild-type strains henceforth, see Supplementary Methods). These two genes, known targets of the pheromone pathway[1,6], were selected as indicators of a more general gene expression response to pheromone. To exclude the effects of possible gradient variability between different chambers, we analysed Fus1–EGFP expression levels of cells in multicellular clusters (4–15 cells) with c_{ph} variation <5 nM across a cluster (Fig. 2a). (The same c_{ph} was assigned to all cells within one cluster for all further analysis.) At $c_{ph} = 20$–50 nM, cells within one cluster frequently exhibited different phenotypic responses uncorrelated with their positions in the cluster. In the same c_{ph} range, there was clear bimodality in the expression of Fus1–EGFP in individual cells (Fig. 2a; Supplementary Fig. 4). The fluorescence intensity of membrane-localized Fus1–EGFP measured with an epi-fluorescence microscope (as in Fig. 2a) correlated well with the total membrane-localized fluorescence estimated by confocal imaging (Supplementary Information and Supplementary Fig. 4). We subdivided cell clusters into groups of cells (4–11 cells per group) displaying one of the BUD/CCA/SHM/RFS phenotypes and explored the correlation between phenotype and gene expression. Strikingly, differences in Fus1–EGFP expression levels between BUD, CCA and RFS cells were insignificant, whereas the difference between SHM cells and cells of all other phenotypes was markedly significant (Fig. 2a). The dose response for Fus3–EGFP expression was qualitatively similar, but the bimodality was much less prominent (Supplementary Fig. 5).

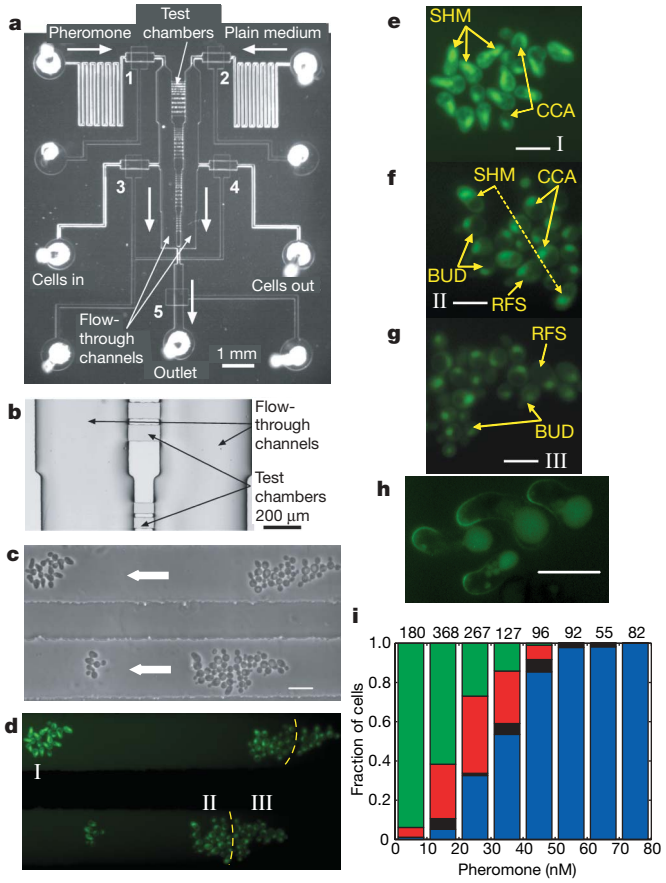

Figure 1 | Pheromone dose–response analysis using a microfluidic experimental setup. **a**, The microfluidic device consists of two layers of microchannels: a flow layer (labelled inlets) of flow-through channels and test chambers and a control layer, with 5 membrane valves[30] (numbered 1–5) actuated from 4 separate control inlets (not labelled). **b**, Magnified view of an area with two 25-μm-deep flow-through channels (wide vertical strips) and 5-μm-deep test chambers between them (see Supplementary Information for details). **c**, **d**, Phase contrast and fluorescence microscopy images of two adjacent chambers with Fus3–EGFP cells six hours after pheromone exposure. (c_{ph} in the field of view increases from right to left, from 10 to 50 nM). Yellow dashed lines indicate boundaries between cell clusters merged owing to cell division. Arrows in **c** denote the direction of increasing pheromone (see Supplementary Fig. 2 for gradient image). **e**–**g**, Close-up Fus3–EGFP fluorescence images of cell clusters I, II and III displaying mixtures of different phenotypes. **h**, Fus1–EGFP expressing cells displaying chemotropism in a similar chamber. Scale bars are 20 μm (**c**, **d**), 10 μm (**e**–**g**) and 5 μm (**h**). **i**, Fraction of different phenotypes of wild-type cells six hours after pheromone exposure. Phenotypes are colour coded as: BUD (green); CCA (red); RFS (black); and SHM (blue). Numbers on the top are the total numbers of cells in the bins.

Mathematical model for transcriptional regulation

The phenotype co-existence and bimodality in Fus1–EGFP and Fus3–EGFP expression indicated that the underlying gene regulation network might exhibit at least two distinct stable states (bistability). Many natural and engineered biochemical networks can exhibit bistability or multistability, usually as a consequence of one or more positive feedback interactions[7–14]. Deterministic bistable systems eventually converge to one of the two distinct steady states available under a given constant input, where the chosen steady state is determined by the system's history (hysteresis). Such systems produce histograms with unimodal distributions. In contrast, a combination of bistability with inherent stochastic noise might allow the system to switch between the two stable steady states, resulting in co-existence of two discrete response levels in cell populations exposed to the same level of stimulus, that is, response bimodality[3,15]. To investigate possible mechanisms of bistability in the pheromone pathway, we constructed a mathematical model incorporating the activity of the MAPKs Fus3 and Kss1, the pheromone-response specific transcription factor Ste12, and upregulation in expression of *FUS1, FUS3* and *STE12* by activated Ste12 (refs 1 and 6; Fig. 3a; Supplementary Figs 8–15). Unphosphorylated Kss1 exerts an inhibitory effect on the

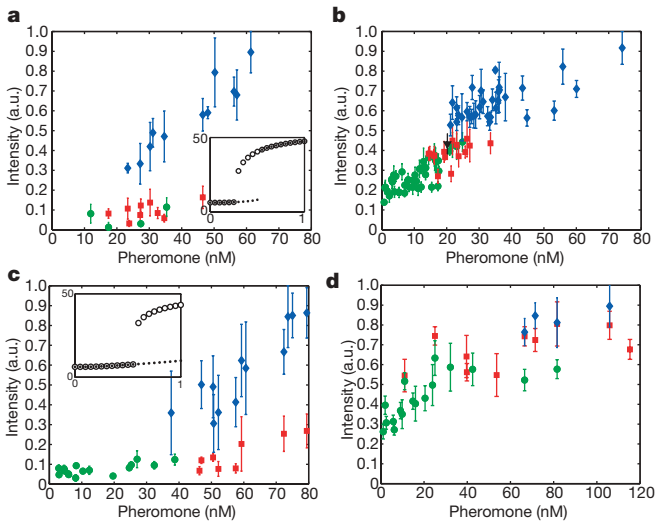

Figure 2 | Quantification of Fus1 protein and gene expression. **a**, Membrane-localized Fus1–EGFP in wild type (strain AL4). **b**, YFP driven by the *FUS1* promoter in wild type (strain SP42). **c**, Membrane-localized Fus1–EGFP in a $PSTE12_{3PREmut}$ strain (strain ZH579). **d**, YFP driven by the *FUS1* promoter in *fus3Δ* (strain SP44). The data (mean ± s.d.) from different cell groups ($n = 4$–11 cells, cell groups with $n < 4$ cells are neglected) are colour-coded as in Fig. 1i: BUD (green circles), CCA (red squares), RFS (black triangles) and SHM (blue diamonds). Fluorescence intensities are normalized so that the maximal (mean + s.d.) value in each experiment corresponds to unity. Insets in **a** and **c** are the corresponding predictions of the model (see also Supplementary Fig. 11). Expression levels of SHM and CCA cells in the region of co-existence are significantly different according to a two-sample *t*-test (assuming a two-tailed distribution and unequal variances): $P = 2.6 \times 10^{-4}$ for **a**; $P = 6.3 \times 10^{-6}$ for **b**; and $P = 1.1 \times 10^{-5}$ for **c**. a.u., arbitrary units.

pathway by binding to Ste12 and potentiating Dig1,2-mediated repression of Ste12 (ref. 16), whereas phosphorylated Fus3 and Kss1 can activate Ste12 thus enhancing the pathway activation[16–18]. Therefore, the model included activation of Ste12 by phosphorylated Fus3 and Kss1, and repression of Ste12 by unphosphorylated Kss1. The model generated *FUS1* and *FUS3* transcription dose–response curves with a combination of monostable and bistable regions (Figs 2a and 3b, insets; Supplementary Fig. 5d), thus reproducing the experimentally observed dose–response curves.

The bimodal expression of Fus1–EGFP and Fus3–EGFP (Fig. 2a; Supplementary Fig. 5a) suggested substantial stochastic variation in the concentrations of key pheromone pathway molecules across the cell population. Cell–cell differences in the signalling pathway components can be a significant source of variation in the pheromone response, especially at low pheromone concentrations[19]. Stochastic variability is also likely to diminish the effect of hysteresis in a bistable system[15]. Indeed, we did not observe any significant hysteretic effects in the response (Supplementary Figs 3 and 5b).

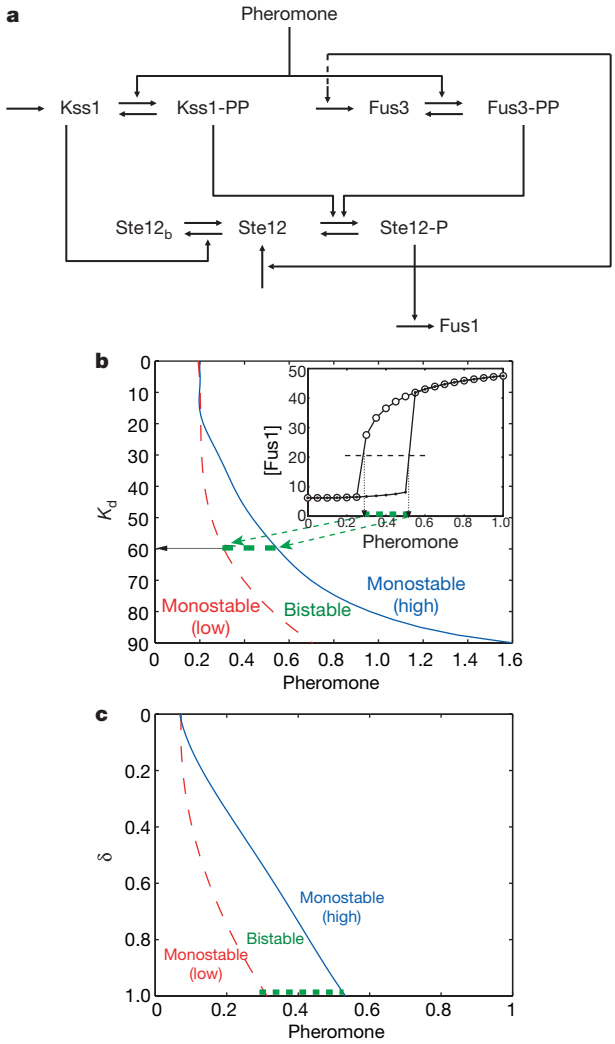

Figure 3 | Computational modelling of transcriptional regulation in the pheromone response. **a**, A simplified diagram of signalling and transcriptional regulation in the pheromone pathway. 'P' denotes phosphorylated forms of the species. $Ste12_b$ denotes the Kss1-bound repressed Ste12. **b**, Ste12 autoregulation is a critical determinant of bistability in the model. For each binding constant K_d of Ste12-P to the *STE12* promoter, the bistability region is confined between the red and blue curves. The inset shows the hysteretic dependence of [Fus1] (a.u.) on pheromone (a.u.) for nominal K_d. a.u., arbitrary units. Dashed green lines in the inset and **b** and **c** indicate the bistability ranges for nominal K_d. Filled and open circles in the inset correspond to low and high initial concentrations of the relevant species, respectively (Supplementary Table 1 and 2). **c**, Plot similar to **b** shows the region of bistability for various values of normalized Kss1 expression (δ). $\delta = 1$ corresponds to the wild-type case and $\delta = 0$ to the *kss1*Δ case (see Supplementary Information for a model description).

Transcriptional regulation: roles of MAPKs and Ste12

To verify that the bistability is regulated at the transcriptional level, as suggested by the model, we studied cells expressing yellow fluorescent protein (YFP) under the control of the *FUS1* promoter (also referred to as a wild-type strain, see Supplementary Methods). These cells gave a bimodal distribution of fluorescence intensity (Fig. 2b), which was qualitatively similar to but less pronounced than that of the Fus1–EGFP cells (see Supplementary Information for a discussion).

Analysis of the model further suggested that the nonlinear transcriptional autoregulation of Ste12 is essential for the bistable response. To investigate this, we mutated the three consensus pheromone response element (PRE) sequences in the promoter region upstream of *STE12* ($PSTE12_{3PREmut}$), leaving only non-consensus sites available for binding by activated Ste12 (Supplementary Information). We modelled this mutation by increasing K_d of Ste12 binding, which resulted in the bistability region moving to higher c_{ph} and becoming wider (Figs 2c, inset, and 3b; Supplementary Figs 11d and 12i). Both effects were observed experimentally, with the CCA phenotype in mutated cells found at much higher c_{ph} than in wild-type cells (Fig. 2c).

To investigate the respective roles of Fus3 and Kss1, we first analysed *fus3*Δ cells. Shmooing and polarized growth were severely hampered, occurring at much higher c_{ph} (Fig. 2d; Supplementary Figs 6 and 7), in agreement with previous studies that have highlighted the importance of Fus3 for the mating response[20–22]. Up to the highest c_{ph} tested ($c_{ph} > 100$ nM), these cells displayed a mixture of different phenotypes. We also observed hyperinvasive growth at low c_{ph}[18,23], and a moderate increase in the *FUS1*-promoter-driven transcription over the entire pheromone range. Results of the mathematical model agreed with the experiments regarding the important role of Fus3 in the pathway response (Supplementary Fig. 9).

To study the role of Kss1, we evaluated Fus1–EGFP expression (Fig. 4a) and *FUS1*-promoter-driven transcription (Fig. 4b) in *kss1*Δ cells as functions of c_{ph}. The model predicted substantial reduction of bistability in these cells, which was expected to lead to reduced bimodality in Fus1–EGFP expression. Additionally, knocking out *KSS1* was expected to reduce the c_{ph} at which *FUS1* expression starts to increase and saturate (Fig. 3c; Supplementary Figs 10 and 11a). In close agreement with the model, bimodality in gene expression in *kss1*Δ cells was drastically reduced, and the pheromone sensitivity saturated at substantially lower c_{ph}. Strikingly, in contrast to wild-type cells, the levels of gene expression in Kss1-deficient BUD and CCA cells were highly sensitive to variation in c_{ph}, whereas in SHM cells gene expression was essentially saturated (compare Fig. 2a, b with Fig. 4a, b). The increased activation of BUD cells is consistent with previously observed Fus1 upregulation without concomitant cell cycle arrest in *kss1*Δ cells[21].

We predicted that the graded increase of Fus1–EGFP expression in wild-type SHM cells was closely connected to pheromone-dependent phosphorylation of Kss1, leading to gradual reduction in Kss1-mediated repression of Ste12 (ref. 24). To test this hypothesis, we transformed Fus1–EGFP expressing *kss1*Δ cells either with the YCpU-*kss1*(AEF) or the YCpU-*kss1*(Y24F) plasmids[16,24,25]. $Kss1_{AEF}$ cannot be phosphorylated by the MAPKK Ste7, and hence lacks kinase activity. $Kss1_{Y24F}$ can be phosphorylated by Ste7 to the same level as wild-type, but its phosphorylated form lacks kinase activity. Unlike in *kss1*Δ cells, in both mutants, CCA cells showed only a modest increase in gene transcription, which was probably a consequence of repression of Ste12 by unphosphorylated $Kss1_{Y24F}$ and $Kss1_{AEF}$, which acted similarly to unphosphorylated Kss1 in wild-type cells. The bimodality and the growth of Fus1–EGFP expression with c_{ph} in $Kss1_{Y24F}$ SHM

cells were both similar to those in wild-type cells, indicating that the kinase activity of phosphorylated Kss1 is not essential for the observed behaviours (Fig. 4c). In contrast, the $Kss1_{AEF}$ mutant showed a stronger bimodality than wild type (Fig. 4d), and unlike wild-type SHM cells, $Kss1_{AEF}$ SHM cells showed no appreciable enhancement of Fus1–EGFP expression with increasing c_{ph}. This behaviour is predicted by the model: since Ste7 does not phosphorylate $Kss1_{AEF}$, the repression of Ste12 by $Kss1_{AEF}$ is not likely to be weakened with increasing c_{ph}. All major trends in Kss1 mutants were consistent with mathematical model predictions (Fig. 4 and Supplementary Fig. 11).

Gradient sensing of wild-type and *kss1*Δ cells

Our observations of wild-type SHM cells indicated that, as expected, the mating projections were predominantly oriented in the direction of increasing c_{ph}. Gradient sensing was strongest at lower c_{ph}, whereas, at higher c_{ph}, the orientation of projections became increasingly random. Interestingly, the c_{ph} range of gradient sensitivity seemed to coincide with the range of sensitivity of *FUS1* expression to variation of c_{ph}. Pheromone dependence of *FUS1* expression may be representative of a large subset of genes, some of which are likely to be essential for gradient sensing. Hence, we proposed that the c_{ph} sensitivity of gene expression reflects sensitivity of the signalling apparatus necessary for precise gradient sensing. Accordingly, the saturated *FUS1* expression in SHM *kss1*Δ cells might coincide with impaired gradient sensitivity. Therefore, we used the microfluidic device to further examine gradient sensing in wild-type and *kss1*Δ cells.

We found (Fig. 5a, d, e, h, i) that the directional bias in wild-type cells increased significantly with time, in general agreement with previous reports[26]. Moreover, the highest gradient sensitivity was consistently observed at high values of the gradient, $\gamma = \partial c_{ph}/\partial x$ and low c_{ph}. We quantified the precision of gradient sensing within a cluster of cells (4–11 SHM cells) by a parameter σ, the root mean square of the angles between the observed projections in the cluster and the direction of the gradient (precision decreases with increasing σ). σ values were binned into two equal intervals, 0–55° and 55–110°, covering the whole experimental range, and were plotted on the c_{ph}–γ plane, with bin-specific symbols (Fig. 5f). The results suggested a linear relationship between the γ and c_{ph} values for cell clusters having the same range of σ, that is $\gamma = \rho \cdot (c_{ph} - c_0) + \gamma_0$, where γ_0 and c_0 are constant and ρ is different for the two sets of cell clusters. We notice that $c_0 \approx 15$–20 nM, the value of c_{ph} where the two linear regression lines intersect, is also the lowest concentration at which SHM cells are observed. σ remained constant at constant fractional gradient, $\rho = (\gamma - \gamma_0)/(c_{ph} - c_0)$, and more precise gradient sensing (lower σ) corresponded to larger ρ (Fig. 5f). These findings suggest that yeast cells respond to the fractional rather than absolute gradient of pheromone, and that gradient sensing in yeast is optimized for exponential concentration profiles (see Supplementary Information). The sensitivity to the fractional gradient of a chemical cue is in surprising agreement with the results reported for gradient sensing by the amoeba *Dictyostelium discoideum* and grasshopper neurons[27,28].

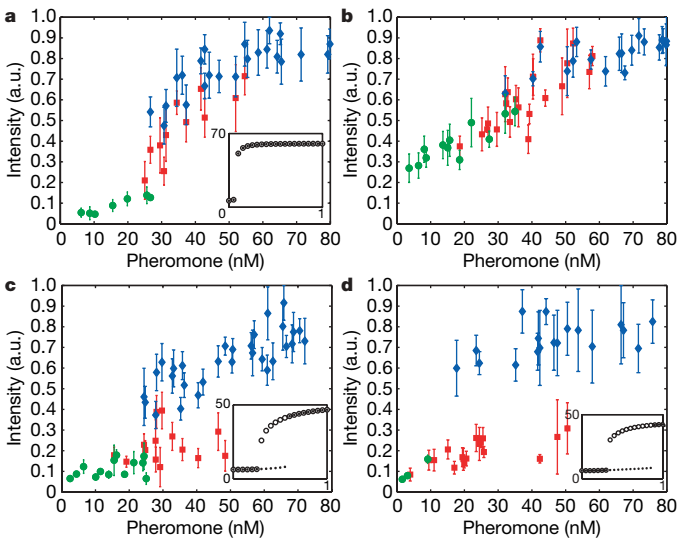

Figure 4 | Role of Kss1 in regulating the pheromone response. **a**, **b**, *kss1*Δ cells expressing Fus1–EGFP (ZH552) (**a**) and YFP driven by the *FUS1* promoter (SP43) (**b**) were exposed to the same conditions as in Fig. 2. Similar experiments were performed with a YCpU-*kss1*(Y24F) plasmid (**c**) and a YCpU-*kss1*(AEF) plasmid (**d**) introduced into the Fus1–EGFP *kss1*Δ strain used in **a**. Fluorescence intensities are normalized and plotted (mean ± s.d.) as in Fig. 2. a.u., arbitrary units. Insets (**a**, **c**, **d**) are the predictions of the mathematical model for the corresponding strains (see also Supplementary Fig. 11). *P*-values (calculated as in Fig. 2) were 1.0×10^{-8} for **c** and 3.2×10^{-11} for **d** indicating significant difference in expression levels of SHM and CCA cells. In contrast, this difference was relatively insignificant in **a** with a *P*-value of 0.017 and was insignificant in **b** with a *P*-value of 0.35.

Sensitivity of cells to fractional gradients further implies that gradient sensing can dramatically deteriorate at higher pheromone concentrations. We observed this deterioration in both wild-type and *kss1*Δ cells, but in *kss1*Δ cells it occurred at substantially lower c_{ph} than in wild type (Fig. 5g). Therefore, deficiency in Kss1 leads to a decrease in the range of c_{ph} in which gradient sensing is efficient, just as predicted above. Similarly, we observe that wild-type cells sense gradients substantially better than *kss1*Δ cells by comparing their values of σ for different ratios of γ to c_{ph} (Fig. 5i). Interestingly, wild-type cells performed only marginally better than *kss1*Δ cells in terms of the initial projection direction, but showed markedly better alignment along the gradient over time as compared to *kss1*Δ cells (Fig. 5h–i). It thus seems that the progressive improvement in gradient sensing in wild-type SHM cells is strongly correlated with the sensitivity of pheromone-induced gene expression to variation of c_{ph}. We also studied the gradient sensing of the strain containing the *STE12* promoter with three mutated consensus PRE sites (Supplementary Fig. 16), as well as the two Kss1 mutant strains, $Kss1_{Y24F}$ and $Kss1_{AEF}$ (Supplementary Fig. 17). In all cases, the existence of an extended dynamic range of gradient sensing was correlated with the c_{ph} sensitivity of the pheromone-induced gene expression in SHM cells.

Conclusions

This study yielded several important insights into the physiology of pheromone response in *S. cerevisiae*. The observed combination of switch-like and graded dose responses, combined with stochastic variability across a cell population, can provide significant benefits for mating yeast populations. First, bimodality in gene expression allows a cell population to diversify its transcriptional response at relatively low pheromone concentrations, reducing the cost of possible inappropriate engagement in expensive pheromone-dependent gene amplification. Thus, when exposed to weak pheromone signals, some cells continue to suppress the pheromone response, whereas others display amplified gene expression correlated with the formation of mating projections. These shmooing cells, capable of sensing fractional pheromone gradients, benefit from the particularly high gradient-sensitivity that we observe at low c_{ph} (higher fractional gradient). Second, continued sensitivity of gene expression in shmooing cells to increasing c_{ph} seems to extend the c_{ph} range in which cells can sense gradients. Thus, as cells approach the mating partner, they can adjust to increasing pheromone concentrations with only partial compromise of gradient sensing. Strikingly, many features of the wild-type pheromone response, including bimodality in gene expression and high dynamic range of gradient sensing, are critically dependent on the presence of Kss1. In particular, the switch-like increase of gene expression in shmooing cells is a result of the combined effect of Ste12 repression by unphosphorylated Kss1 and of Ste12 autoregulation. The graded increase of gene expression with increasing c_{ph} depends on pheromone-regulated phosphorylation of

Kss1, which results in graded reduction in Kss1-mediated repression of Ste12, and possibly, on the ability of phosphorylated MAPKs to activate the pathway. A reduction in the graded increase of gene expression in *kss1*Δ cells correlates with lower precision and reduced dynamic range of gradient sensing. Our results suggest that the role of Kss1 is not redundant with that of Fus3, and provide functional significance for the strong negative regulation exerted by inactive Kss1 on Ste12, the transcriptional factor essential for the pheromone response.

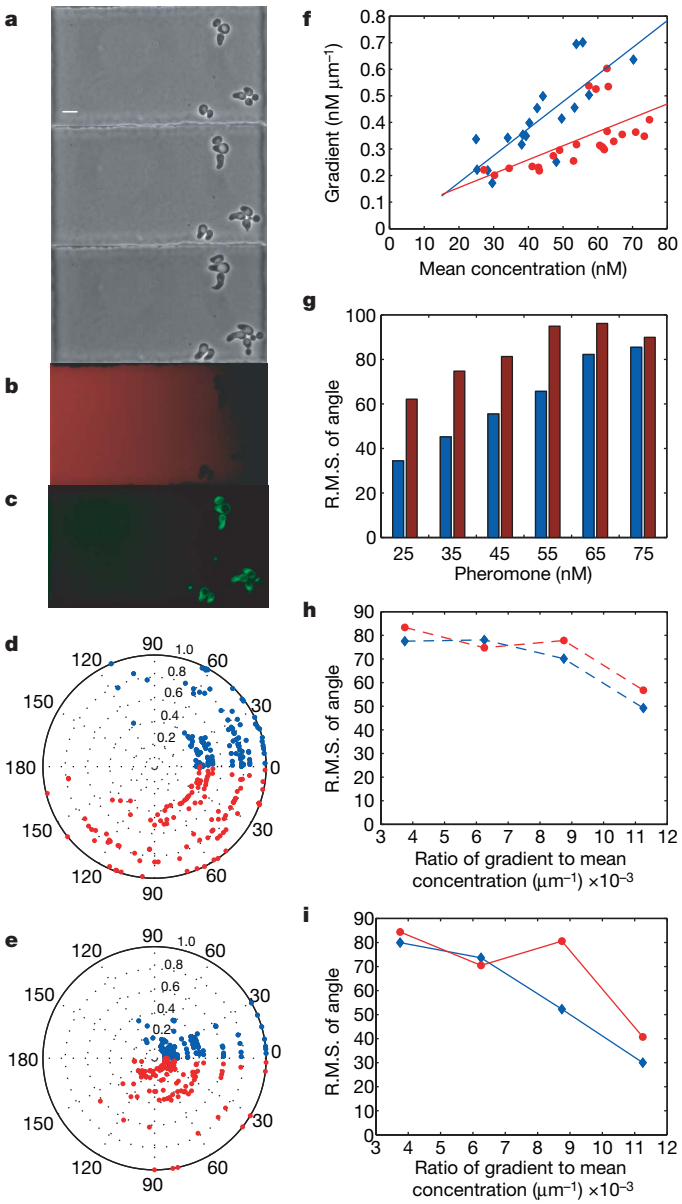

Figure 5 | Quantification of pheromone gradient sensing. a, Chemotropism at 4, 5 and 7 hours (top to bottom) following exposure to a pheromone gradient (scale bar, 10 μm). **b**, **c**, c_{ph} profile (visualized with Alexa Fluor 555 dye) and Fus3–EGFP, respectively, at 5 hours. **d**, **e**, Polar plots representing the dependence of the absolute value of the angle between individual cell projections and the gradient, on c_{ph} (radial dimension in **d**) and γ (radial dimension in **e**), normalized to the maximal values of c_{ph} and γ, respectively. Data are shown for the same cells at 4 hours (red) and 20 h (blue) post-stimulation. **f**, Cell clusters with $\sigma = 0–55^{\circ}$ and $\sigma = 55–110^{\circ}$ are plotted in the c_{ph}–γ plane in blue and red, respectively (σ is the root mean square, R.M.S., of the angle between the projection and the gradient direction); $n = 4–11$ SHM cells per cluster. Straight lines are the corresponding linear regression lines $R^2 = 0.64$ (blue) and $R^2 = 0.38$ (red). **g–i**, σ displayed by groups of SHM cells in wild-type (blue) and *kss1*Δ (red) backgrounds at $t = 4$ hours in **h** and $t = 9$ hours in **g** and **i**, as a function of the c_{ph} (**g**) and γ / c_{ph} (**h–i**). Each bar (or point) represents at least 5 clusters of SHM cells. Bars in (**g**) correspond to 10 nM widths in c_{ph}. Points in **h**, **i** represent bin widths of 0.0025 μm^{-1} in γ / c_{ph}.

METHODS

Yeast and nucleic acid manipulations were performed as previously described[29]. Details on strain construction are present in the Supplementary Information. Fabrication and operation of the microfluidic device is described in detail in Supplementary Information. Evaluation of the pheromone concentrations and gradients, and of the levels of fluorescent reporter expression was performed using custom-written Matlab programs (See Supplementary Information for details). Mathematical model simulations were run in Matlab.

Received 20 June; accepted 21 December 2006.
Published online 18 February 2007.

1. Roberts, C. J. *et al.* Signaling and circuitry of multiple MAPK pathways revealed by a matrix of global gene expression profiles. *Science* **287,** 873–880 (2000).
2. Poritz, M. A., Malmstrom, S., Kim, M. K., Rossmeissl, P. J. & Kamb, A. Graded mode of transcriptional induction in yeast pheromone signalling revealed by single-cell analysis. *Yeast* **18,** 1331–1338 (2001).
3. Ferrell, J. E. Jr & Machleder, E. M. The biochemical basis of an all-or-none cell fate switch in *Xenopus* oocytes. *Science* **280,** 895–898 (1998).
4. Jeon, N. L. *et al.* Neutrophil chemotaxis in linear and complex gradients of interleukin-8 formed in a microfabricated device. *Nature Biotechnol.* **20,** 826–830 (2002).
5. Moore, S. A. Comparison of dose–response curves for alpha factor-induced cell division arrest, agglutination, and projection formation of yeast cells. Implication for the mechanism of alpha factor action. *J. Biol. Chem.* **258,** 13849–13856 (1983).
6. Lee, T. I. *et al.* Transcriptional regulatory networks in *Saccharomyces cerevisiae*. *Science* **298,** 799–804 (2002).
7. Angeli, D., Ferrell, J. E. Jr & Sontag, E. D. Detection of multistability, bifurcations, and hysteresis in a large class of biological positive-feedback systems. *Proc. Natl Acad. Sci. USA* **101,** 1822–1827 (2004).
8. Becskei, A., Seraphin, B. & Serrano, L. Positive feedback in eukaryotic gene networks: cell differentiation by graded to binary response conversion. *EMBO J.* **20,** 2528–2535 (2001).
9. Biggar, S. R. & Crabtree, G. R. Cell signaling can direct either binary or graded transcriptional responses. *EMBO J.* **20,** 3167–3176 (2001).
10. Ferrell, J. E. Jr. Self-perpetuating states in signal transduction: positive feedback, double-negative feedback and bistability. *Curr. Opin. Cell Biol.* **14,** 140–148 (2002).
11. Gardner, T. S., Cantor, C. R. & Collins, J. J. Construction of a genetic toggle switch in *Escherichia coli*. *Nature* **403,** 339–342 (2000).
12. Ninfa, A. J. & Mayo, A. E. Hysteresis vs. graded responses: the connections make all the difference. *Sci. STKE* **232,** pe20 (2004).
13. Pomerening, J. R., Sontag, E. D. & Ferrell, J. E. Jr. Building a cell cycle oscillator: hysteresis and bistability in the activation of Cdc2. *Nature Cell Biol.* **5,** 346–351 (2003).
14. Sha, W. *et al.* From the cover: hysteresis drives cell-cycle transitions in *Xenopus laevis* egg extracts. *Proc. Natl Acad. Sci. USA* **100,** 975–980 (2003).
15. Ozbudak, E. M., Thattai, M., Lim, H. N., Shraiman, B. I. & Van Oudenaarden, A. Multistability in the lactose utilization network of *Escherichia coli*. *Nature* **427,** 737–740 (2004).
16. Bardwell, L., Cook, J. G., Zhu-Shimoni, J. X., Voora, D. & Thorner, J. Differential regulation of transcription: repression by unactivated mitogen-activated protein kinase Kss1 requires the Dig1 and Dig2 proteins. *Proc. Natl Acad. Sci. USA* **95,** 15400–15405 (1998).
17. Cook, J. G., Bardwell, L. & Thorner, J. Inhibitory and activating functions for MAPK Kss1 in the *S. cerevisiae* filamentous-growth signalling pathway. *Nature* **390,** 85–88 (1997).
18. Madhani, H. D., Styles, C. A. & Fink, G. R. MAP kinases with distinct inhibitory functions impart signaling specificity during yeast differentiation. *Cell* **91,** 673–684 (1997).
19. Colman-Lerner, A. *et al.* Regulated cell-to-cell variation in a cell-fate decision system. *Nature* **437,** 699–706 (2005); erratum *Nature* **439,** 502 (2006).
20. Elion, E. A., Satterberg, B. & Kranz, J. E. FUS3 phosphorylates multiple components of the mating signal transduction cascade: evidence for STE12 and FAR1. *Mol. Biol. Cell* **4,** 495–510 (1993).
21. Farley, F. W., Satterberg, B., Goldsmith, E. J. & Elion, E. A. Relative dependence of different outputs of the *Saccharomyces cerevisiae* pheromone response pathway on the MAP kinase Fus3p. *Genetics* **151,** 1425–1444 (1999).
22. Matheos, D., Metodiev, M., Muller, E., Stone, D. & Rose, M. D. Pheromone-induced polarization is dependent on the Fus3p MAPK acting through the formin Bni1p. *J. Cell Biol.* **165,** 99–109 (2004).
23. Roberts, R. L. & Fink, G. R. Elements of a single MAP kinase cascade in *Saccharomyces cerevisiae* mediate two developmental programs in the same cell type: mating and invasive growth. *Genes Dev.* **8,** 2974–2985 (1994).

24. Bardwell, L. *et al.* Repression of yeast Ste12 transcription factor by direct binding of unphosphorylated Kss1 MAPK and its regulation by the Ste7 MEK. *Genes Dev.* **12,** 2887–2898 (1998).
25. Ma, D., Cook, J. G. & Thorner, J. Phosphorylation and localization of Kss1, a MAP kinase of the *Saccharomyces cerevisiae* pheromone response pathway. *Mol. Biol. Cell* **6,** 889–909 (1995).
26. Segall, J. E. Polarization of yeast cells in spatial gradients of alpha mating factor. *Proc. Natl Acad. Sci. USA* **90,** 8332–8336 (1993).
27. Janetopoulos, C., Ma, L., Devreotes, P. N. & Iglesias, P. A. Chemoattractant-induced phosphatidylinositol 3,4,5-trisphosphate accumulation is spatially amplified and adapts, independent of the actin cytoskeleton. *Proc. Natl Acad. Sci. USA* **101,** 8951–8956 (2004).
28. Isbister, C. M., Mackenzie, P. J., To, K. C. W. & O'Connor, T. P. Gradient steepness influences the pathfinding decisions of neuronal growth cones *in vivo*. *J. Neurosci.* **23,** 193–202 (2003).
29. Guthrie, C. & Fink, G. R. (eds) *Methods in Enzymology. Guide to Yeast Genetics and Molecular Biology* (Academic, San Diego, 1991).
30. Unger, M. A., Chou, H. P., Thorsen, T., Scherer, A. & Quake, S. R. Monolithic microfabricated valves and pumps by multilayer soft lithography. *Science* **288,** 113–116 (2000).

Supplementary Information is linked to the online version of the paper at www.nature.com/nature.

Acknowledgements The authors would like to thank M. Piel from A. Murray's laboratory (Harvard) for the initial suggestion of the possible importance of Kss1 in controlling bimodality of pheromone response. They also want to thank P. Sternberg, J. Bruck, M. Peter, A. Colman-Lerner, J. Boeke, L. Bardwell and S. Quake for intellectual and material support of the study. This work was supported by NIH and NSF grants.

Author Contributions S.P., A.G. and A.L. conceived the framework of and wrote the paper, and A.L. oversaw the complete project. A.G., K.C., S.P. and A.L. conceptualized the microfluidic device design and the experimental setup, and K.C. and A.G. fabricated the devices. S.P., P.A.I. and A.L. were involved in the mathematical model setup. Z.H., S.P. and A.L. designed the yeast strains used in the study. S.P. performed the experiments, analysis of results and mathematical model simulations.

Author Information Reprints and permissions information is available at www.nature.com/reprints. The authors declare no competing financial interests. Correspondence and requests for materials should be addressed to A.L. (alev@jhu.edu) and A.G. (agroisman@ucsd.edu).